Available online at www.sciencedirect.com
SCIENCE DIRECT
Journal of Solid State Chemistry 179 (2006) 1183–1191
JOURNAL OF SOLID STATE CHEMISTRY
www.elsevier.com/locate/jssc

$Ag_{1/8}Pr_{5/8}MoO_4$: An incommensurately modulated scheelite-type structure

Vladimir A. Morozov[a,b], Andrei V. Mironov[a], Bogdan I. Lazoryak[a], Elena G. Khaikina[c], Olga M. Basovich[c], Marta D. Rossell[b], Gustaaf Van Tendeloo[b,*]

[a]*Department of Chemistry, Moscow State University, 119899 Moscow, Russia*
[b]*EMAT, University of Antwerp, Groenenborgerlaan 171, B-2020, Antwerp, Belgium*
[c]*Baikal Institute of Nature Management, Siberian Branch of Russian Academy of Science, 670047 Ulan-Ude, Russia*

Received 21 October 2005; received in revised form 20 December 2005; accepted 30 December 2005
Available online 7 February 2006

Abstract

The crystal structure of a complex molybdenum oxide $Ag_{1/8}Pr_{5/8}MoO_4$ is reported. The $Ag_{1/8}Pr_{5/8}MoO_4$ sub-structure can be described on the base of the scheelite ($CaWO_4$) structure. Transmission electron microscopy reveals that the real structure is better described in a (3 + 1)D formalism. According to electron diffraction study the new scheelite-type complex oxide $Ag_{1/8}Pr_{5/8}MoO_4$ crystallizes in the $B2/b(\alpha\beta0)00$ (3 + 1)D superspace group with unit cell parameters $a \approx 7.50$ Å, $b \approx 5.30$ Å, $c \approx 11.74$ Å and $\gamma \approx 135^\circ$ ($Z = 4$) and modulation vector $\mathbf{q} = 0.56\mathbf{a}^* + 0.59\mathbf{b}^*$. The structure of $Ag_{1/8}Pr_{5/8}MoO_4$ is refined from X-ray powder data in the scheelite setting $I2/b(\alpha\beta0)$ with $a = b = 5.3013(4)$ Å, $c = 11.7407(11)$ Å, $\mathbf{q} = 1.14690(14)\mathbf{a}^* + 0.58921(12)\mathbf{b}^*$ with fixed $\gamma = 90^\circ$ angle ($R_p = 0.033$, $R = 0.033$, $R_m = 0.029$, $R_1 = 0.047$, $S = 1.36$). Displacement modulations apply for all atoms. The occupancy modulation shows that one-fourth of the Ag/Pr atoms are absent. The structure can be considered as a crystallographic shear structure with incommensurate ordering of vacancies and displacement modulations for all atoms. The arrangement of Ag/Pr atoms and vacancies is at the origin of the incommensurate modulation in the cation-deficient $Ag_{1/8}Pr_{5/8}MoO_4$ phase.

Keywords: Complex molybdenum oxides; X-ray diffraction; Rietveld refinement

1. Introduction

The study of new advanced materials for optoelectronic applications has attracted many researchers. Recently, increasing attention has been focused on the design and functioning of solid-state lasers [1]. The aim to develop solid-state lasers appears to be important, because they are very useful for many applications, such as medical treatment, industry or optical communication. They are interesting because of their high stability, compactness, high efficiency, long lifetime and low cost. Compounds with the scheelite-type structure can be used as potential laser materials. For example, the scheelite-type $MLn(BO_4)_2$ (M = alkali metal (Li, Na, K), Ln = lanthanides, B = W, Mo) single crystals can be considered as interesting self-doubling solid-state laser host materials. For this reason the optical properties of the scheelite-type compounds have been studied extensively [2].

The $CaWO_4$ scheelite crystallizes in a tetragonal symmetry (S.G. $I4_1/a$) [3]. The scheelite structure is adopted by a large family of compounds with a composition ABO_4. Many different A and B cations with various oxidation states can be easily accommodated in the scheelite structure. Some examples, which demonstrate the ability of the scheelite structure to host the cations with variable oxidation state, are: $KReO_4$ and $AgIO_4$ (A^+ and B^{7+}); $CdMoO_4$ and $CaMoO_4$ (A^{2+} and B^{6+}); $BiVO_4$ and $YNbO_4$ (A^{3+} and B^{5+}); $ZrGeO_4$ (A^{4+} and B^{4+}). The scheelite-type ABO_4 structure is made up of AO_8 polyhedra

*Corresponding author. Fax: +32 3 265 3257.
E-mail address: staf.vantendeloo@ua.ac.be (G. Van Tendeloo).

0022-4596/$ - see front matter © 2006 Elsevier Inc. All rights reserved.
doi:10.1016/j.jssc.2005.12.041

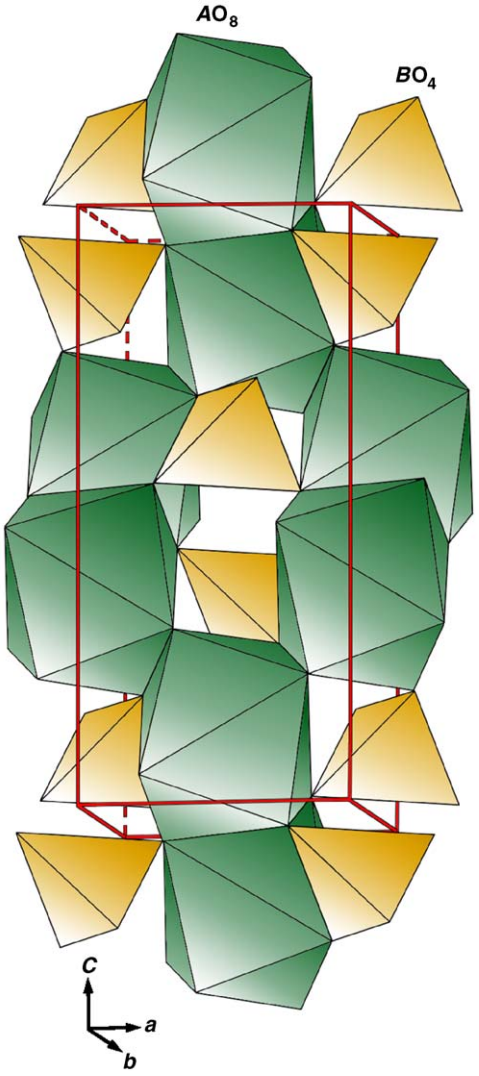

Fig. 1. Polyhedral view of the scheelite-type structure.

and BO_4 tetrahedra connected via common vertices. AO_8 polyhedra connect via the edges and form a 3D framework (Fig. 1).

The Ca^{2+} cations in $CaBO_4$ (B = W, Mo) can be substituted by a combination of a monovalent alkali metal and a trivalent cation according to the formula $MR(BO_4)_2$ (M = alkali metal, R = Ln, Y, Bi). These compounds show a random distribution of M^+ and R^{3+}. Complex molybdenum oxides $MLn(MoO_4)_2$ (M = Li, Na) with the scheelite-type structure are known for all Ln elements [4–6]. Only $LiLa(MoO_4)_2$ undergoes a phase transition from a low-temperature non-scheelite modification to the high-temperature scheelite-type phase [7]. Other $MLn(MoO_4)_2$ (M = Li, Na) compounds do not reveal such polymorphism. Moreover, complex Ln molybdenum oxides $MLn(MoO_4)_2$ were synthesized for other monovalent cations such as Cu^+, Ag^+, and Tl^+ [8–16]. $AgLa(BO_4)_2$ (B = Mo; W) compounds have been first synthesized by Sleight et al. [9] and their catalytic properties have been studied. Later, $AgLn(BO_4)_2$ (B = Mo; W) compounds have been prepared for other R^{3+} elements [10–16]. The structure of $AgLn(MoO_4)_2$ and the high-temperature $AgLn(WO_4)_2$ phase are closely related to the scheelite type with a statistical distribution of Ag^+ and Ln^{3+} cations.

It should be noted that the catalytic properties of the scheelite-type compounds are the second reason for their extensive study. Different complex bismuth molybdenum oxides are known as catalysts for selective oxidation, ammoxidation and oxidative dehydrogenation of olefins to the corresponding aldehydes, nitrides and diolefins [17–20]. Some of these compounds crystallize in the scheelite-type structure.

$Bi_2(MoO_4)_3$ oxide has a monoclinic distorted scheelite-type structure [21]. The substitution of $3Ca^{2+}$ by $2R^{3+}$ (R = Ln and Bi) cations in $CaBO_4$ (B = W, Mo) results in the creation of a cation vacancy (□) in the framework. In this case, the formula of the bismuth molybdenum oxide should be more correctly written as $Bi_{2/3}\square_{1/3}MoO_4$, where one-third of the cation positions is vacant. These cation vacancies in the framework are very important for the catalytic properties of the scheelite-type materials [9,20,22–24]. The ordering of cation vacancies in the scheelite-type structure depends on the kind of A and B elements in the cation sub-structure (Fig. 2) [21,25–27]. The

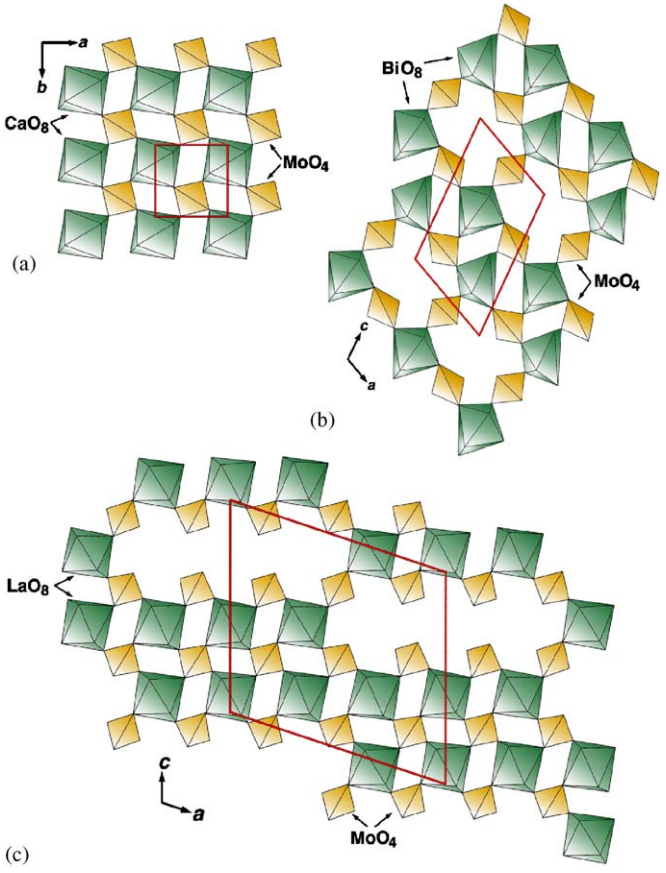

Fig. 2. A layer with AO_8 polyhedra and MoO_4 tetrahedra in the scheelite-type structures: $CaMoO_4$ (a), $Bi_2(MoO_4)_3$ (b) and $La_2(MoO_4)_3$ (c).

existence of scheelite-type compounds with less than one-third of cation vacancies in the structure has been shown before. The investigation of phase formation in the system M_2MoO_4–$Ln_2(MoO_4)_3$ (M = Li, Na) revealed a new scheelite-type phase $M_{1/8}Ln_{5/8}\square_{1/4}MoO_4$ (M:Ln ratio = 1:5) in the region between $MLn(MoO_4)_2$ and $Ln_2(MoO_4)_3$ [28,29]. It should also be pointed out that the formation of the $M_{1/8}Ln_{5/8}\square_{1/4}MoO_4$ phase with a distorted scheelite-type framework is possible only if $Ln_2(MoO_4)_3$ also has the scheelite-type structure. Since double silver and Ln (Ag:Ln ratio = 1:1) molybdates crystallize similar to the $MLn(MoO_4)_2$ (M = Li, Na) phases, the formation of a scheelite-type $Ag_{1/8}Ln_{5/8}\square_{1/4}MoO_4$ phase in some of the Ag_2MoO_4–$Ln_2(MoO_4)_3$ systems can be expected.

In this paper, we present results of the study on an incommensurately modulated scheelite-type structure, $Ag_{1/8}Pr_{5/8}MoO_4$, formed in the system Ag_2MoO_4–$Pr_2(MoO_4)_3$.

2. Experimental

The complex molybdenum oxide $Ag_{1/8}Pr_{5/8}MoO_4$ was prepared from a (1:5) stoichiometric mixture of Ag_2MoO_4 (cubic phase) and $Pr_2(MoO_4)_3$ by a routine ceramic technique at 773–1023 K for 70 h in air followed by quenching from 1023 K to room temperature.

Stoichiometric (2:1) mixtures of $AgNO_3$ (99.99%) and MoO_3 (99.99%), Pr_6O_{11} (99.99%) and MoO_3 (99.99%) have been used for the synthesis of the cubic Ag_2MoO_4 [30,31] and $Pr_2(MoO_4)_3$ precursors, respectively. X-ray diffraction (XRD) powder patterns of $Pr_2(MoO_4)_3$ were similar to the $La_2(MoO_4)_3$ X-ray powder diffraction patterns [25] and did not contain reflections of any foreign phases.

XRD powder patterns (T = 293 K) for the $Ag_{1/8}Pr_{5/8}MoO_4$ crystal structure determination were collected on a STADI-P diffractometer (Cu$K\alpha_1$ radiation, λ = 1.5406 Å, curved Ge monochromator, transmission mode, linear PSD). The data were collected over the range of 10–100° in 2θ with steps of 0.01° 2θ. The Rietveld refinement of the incommensurately modulated structure was performed with the JANA2000 program package [32].

Electron diffraction (ED) and high-resolution electron-microscopy (HREM) investigations were made on crushed samples deposited on holey carbon grids. Energy dispersive X-ray (EDX) analysis and ED patterns were obtained using a Philips CM20 microscope with a LINK-2000 attachment. For the EDX analysis, results were based on the Ag_L, Pr_L and Mo_L lines in the spectra. HREM observations were performed using a JEOL 4000 EX microscope operating at 400 kV. Computer simulations of the HREM images were made using the MacTempas software.

3. Results

3.1. Composition determination

The element composition of $Ag_{1/8}Pr_{5/8}MoO_4$ is confirmed by EDX analysis performed inside the transmission electron microscope together with ED patterns for each crystallite. EDX analysis is carried out at 4 points for 10 different crystallites. The cation ratio is found to be Ag:Pr:Mo = 0.94(6):4.89(19):8.00(17). This is close to the bulk $Ag_{1/8}Pr_{5/8}MoO_4$ composition and reveals a homogenous element distribution in the sample.

3.2. Electron diffraction study

ED patterns of the incommensurately modulated $Ag_{1/8}Pr_{5/8}MoO_4$ are shown in Fig. 3. The most intense reflections are the main reflections and correspond to the scheelite tetragonal $I4_1/a$ subcell with unit cell parameters $a_t \approx 5.30$ Å, $c_t \approx 11.74$ Å. The weaker reflections observed in the [001]* ED pattern are satellite reflections due to an incommensurate modulation of the scheelite-type structure with a modulation vector $\mathbf{q}_t \approx 1.16\mathbf{a}_t^* + 0.59\mathbf{b}_t^*$ (t—tetragonal cell). The two components of the modulation vector require to transform the tetragonal subcell to the monoclinic supercell with unit cell parameters $a \approx a_t \times \sqrt{2} \approx 7.50$ Å, $b \approx a_t \approx 5.30$ Å, $c \approx c_t \approx 11.74$ Å and $\gamma \approx 135°$ and a modulation vector $\mathbf{q}$ having the approximate components $0.56\mathbf{a}^* + 0.59\mathbf{b}^*$.

The indexing of the ED patterns (Fig. 3) was made with four $hklm$ indices given by the diffraction vector

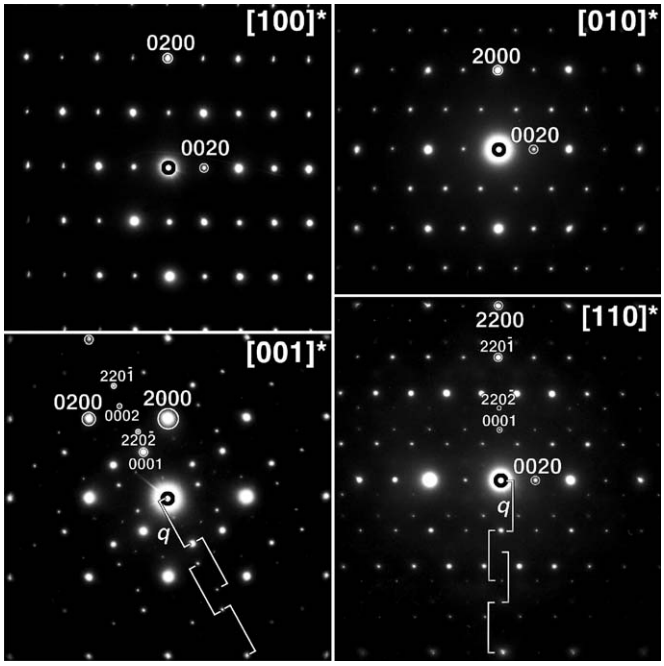

Fig. 3. [100]*, [010]*, [001]* and [110]* ED patterns of the incommensurate modulated $Ag_{1/8}Pr_{5/8}MoO_4$ phase (indexing in the superspace group $B2/b(\alpha\beta0)00$).

$\mathbf{H} = h\mathbf{a}^* + k\mathbf{b}^* + l\mathbf{c}^* + m\mathbf{q}$, $\mathbf{q} \approx 0.56\mathbf{a}^* + 0.59\mathbf{b}^*$. The reflections with $m = 0$ and $m \neq 0$ correspond to the main and satellite reflections, respectively. The ED patterns can be completely indexed in the superspace group $B2/b(\alpha\beta0)00$ with the unique axis c. The superspace group $B2/b(\alpha\beta0)00$ is the conventional standard setting for a superspace group [33]. The [010]*and [100]* diffraction patterns exhibit only main $h\,k\,l\,m$ reflections with $m = 0$. The spots on the [010]* diffraction pattern obey the extinction conditions $h\,0\,l$, $h + l = 2n$ and indicate the possible presence of a B- or I-centered unit cell. In the latter case, reflections on the [100]* pattern should obey the condition $0\,k\,l$, $k + l = 2n$, which is not observed. No other symmetry elements, planes or axis, cannot exist along this direction because of the γ-setting of the monoclinic unit cell. The [100]* pattern exhibits $0\,k\,0\,0$, $k \neq 2n$ reflections forbidden by the $B2/b$ symmetry. The intensity of these reflections, however, is systematically lower than the intensity of the $0\,k\,0\,0$, k—even. On tilting the specimen around the $0\,k\,0$ axis, the reflections $0\,k\,0\,0$, $k =$ odd further weaken and finally vanish in the [001]* pattern. No reflection conditions apply for the satellite reflections besides the B-centering reflection conditions.

3.3. Crystal structure refinement

$Ag_{1/8}Pr_{5/8}MoO_4$ exhibits an incommensurately modulated structure. For such structures, a more elegant description can be obtained using the superspace (3 + 1)D formalism, suggested by De Wolf, Jansen, Janner [34,35]. This superspace formalism allows to recover the lost periodicity via the introduction of one or more additional dimensions, a fourth one in this particular case. Then, the structure regains a periodicity within the (3 + 1)D approach.

The crystal structure of $Ag_{1/8}Pr_{5/8}MoO_4$ is refined by X-ray powder diffraction data using the (3 + 1)D formalism, as it was revealed in the ED investigation. The refinement in the space group $B2/b(\alpha\beta0)00$ converges with $\gamma = 135^\circ$ within the standard deviation, so the final refinement is done for convenience in the $I2/b(\alpha\beta0)00$ space group (unique axis c) with constrained $b = a$ parameters and a fixed $\gamma = 90^\circ$ angle.[1] Two reasons exist for the final refinement of the $Ag_{1/8}Pr_{5/8}MoO_4$ crystal structure in the $I2/b(\alpha\beta0)00$ space group: (1) the standard scheelite setting; and (2) a γ angle very close to 90°. According to one of the standard crystallography rules, if a crystal structure can be described in two or more different monoclinic settings (space group, unit cell parameters, etc.), the setting with minimal deviation of the monoclinic angle from 90° should be chosen.

The fractional coordinates of the $CaWO_4$ type cell (S.G. $I4_1/a$) were used as the initial parameters for the refinement of the average $Ag_{1/8}Pr_{5/8}MoO_4$ structure. The atom coordinates of $CaWO_4$ in the $I4_1/a$ space group model were transformed to a structure model with the space group $I2/b$. The average structure is refined with a random distribution of Ag^+ and Pr^{3+} cations $\left(\frac{1}{8}Ag^+ + \frac{5}{8}Pr^{3+}\right)$ in the A position of the scheelite-type structure with vacancies one-fourth of these A-sites. The refinement of the average $Ag_{1/8}Pr_{5/8}MoO_4$ structure in the isotropic approximation for atomic displacement parameters converges with $R_p = 0.043$, $R_F = 0.036$. Experimental, calculated and difference XRD powder patterns for the average structure are given in Fig. 4. However, the difference XRD powder pattern clearly reveals satellite reflections, which cannot be indexed within the 3D approach.

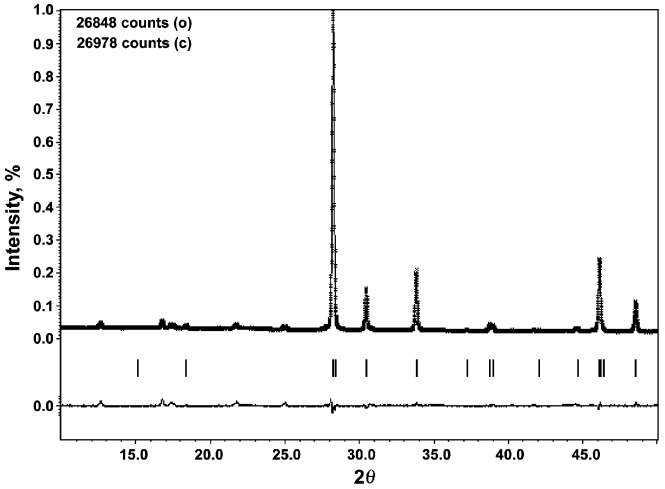

Fig. 4. Fragment of the experimental, calculated and difference XRD powder patterns for the average structure $Ag_{1/8}Pr_{5/8}MoO_4$. Tick marks denote the peak positions of possible main Bragg reflections.

Therefore, one harmonic term of positional modulation parameters for Pr, Mo and oxygen atoms was introduced in the refinement. It converges with negative atomic displacement parameters for the oxygen atoms and unrealistically high modulation parameters. The refinement of the modulation wave parameters for the cations results only in a small displacement modulation (less than 0.17 Å) and a high reliability factor for the first-order satellites $R_p = 0.041$, $R_{Fm} = 0.037$, $R_{F1} = 0.137$ (index m stands for main reflections, 1—for first-order satellites). Then, the difference Fourier map is calculated in the vicinity of the Pr/Ag site (Fig. 5a). The alteration of positive and negative regions suggests to apply a step-like function to the occupational modulation of the Pr/Ag site with $\Delta = 0.75$ and $x_4^0 \approx 0.5$.[2] The following alteration of regions was chosen as starting parameters: Ag ($\Delta = 0.125$ and $x_4^0 = 0.0$), Pr ($\Delta = 0.625$ and $x_4^0 = 0.5$).

A reversed order of Ag and Pr results in slightly worse R-factors and short Pr–O distances and was therefore rejected as well as a random distribution of Pr and Ag over the

[1] The transformation matrix is $T = \begin{pmatrix} 1 & 0 & 0 \\ 1 & 1 & 0 \\ 0 & 0 & 1 \end{pmatrix}$ in the matrix equation $A_{new} = A_{old}T$.

[2] x_4^0—center of the x_4 range, where the atom does exist; Δ—the length of this range. In this case Δ corresponds to the cation fraction on the A-site (6/8).

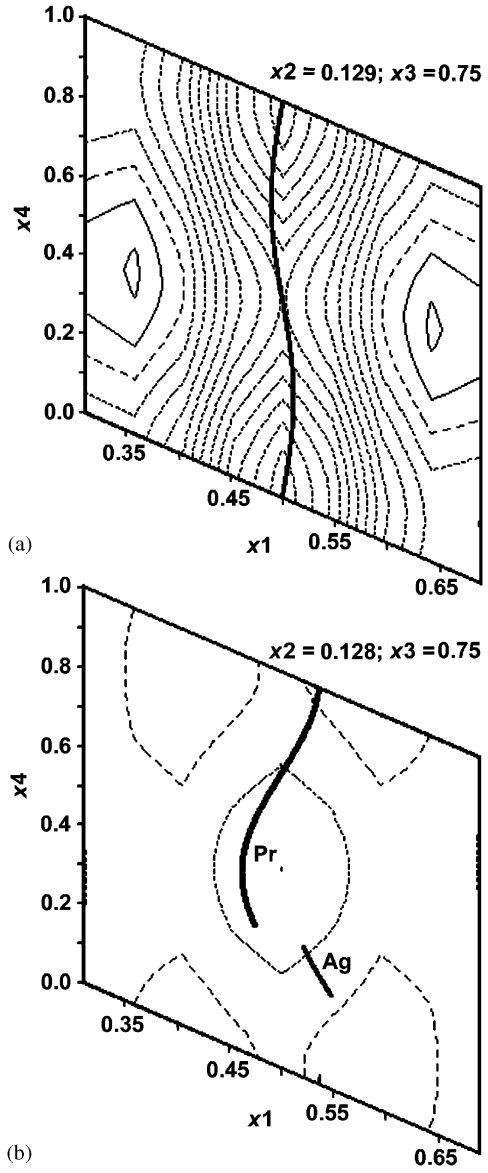

Fig. 5. Difference Fourier map of the Pr/Ag site, x_1–x_4 section. Summation along y and $z \pm 0.6$ Å. (a) The curve corresponds to the displacement modulation of the Pr/Ag site with an occupancy of 3/4 in each unit cell. (b) The curves correspond to the displacement and occupancy modulation of Pr and Ag.

entire cation range ($\Delta = 0.75$) for the same reason. Δ values were fixed according to the EDX analysis and the x_4^0 parameter for Pr was refined; for Ag it was calculated from the corresponding x_4^0 of Pr and Δ values. Such refinement results in a significant reduction of the R-factors down to $R_p = 0.033$, $R_{Fm} = 0.029$, $R_{F1} = 0.046$, Gof = 1.36. Taking into account the Fourier maps and the crystallographic peculiarities of Ag, its x and z coordinates were allowed to refine, but the differences between Ag and Pr coordinates are less than 3σ with the same R-factors, and in the final refinement they were constrained. The difference Fourier map obtained after the occupancy modulation refinement is given in Fig. 5b. Finally, the occupancy modulation of Pr and Ag is presented in Fig. 6. The displacive modulation for the cations significantly reduces and becomes less than 0.11 Å. The refinement of the oxygen displacement modulation results in reasonable atomic displacements. The values of the reliability factors show good agreement between the calculated and experimental profiles. The crystallographic parameters, reliability factors, atomic coordinates, position modulation parameters and the most relevant interatomic distances for $Ag_{1/8}Pr_{5/8}MoO_4$ are listed in Tables 1–4. Experimental, calculated and difference X-ray patterns are given in Fig. 7.

Supplementary material has been sent to the Fachinformationzentrum Karlsruhe, Abt. PROKA, 76344, Eggenstein-Leopoldshaften, Germany, as supplementary material no. 415233 (148pp) and can be obtained by contacting the FIZ (quoting the article details and the corresponding SUP number).

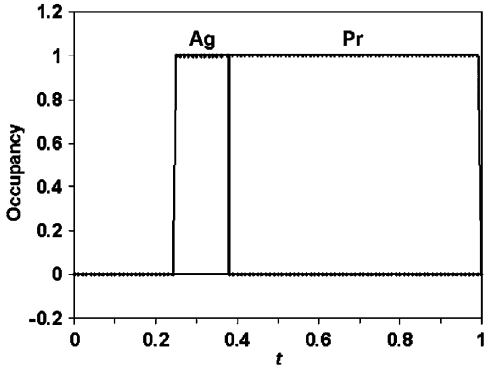

Fig. 6. Ag/Pr and vacancies distribution versus t (phase shift parameter $t = x_4 - \mathbf{q} \cdot \mathbf{r}_i$).

Table 1
Important refined parameters and counting conditions for $Ag_{1/8}Pr_{5/8}MoO_4$

Temperature, K	293
2θ range (°)	10–100
Step scan increment (2θ)	0.01
Radiation (λ, Å)	Cu$K\alpha_1$ (1.5406)
I_{max}	26848
Crystal system	Monoclinic
Space group	$I2/b(\alpha\beta 0)$
Background function	10th-order Legendre polynomial
Profile function	Pseudo-Voigt
No. of refined parameters/refined atomic parameters	51/34
Lattice parameters:	
a (Å)	5.3013(4)
b (Å)	5.3013
c (Å)	11.7407 (11)
γ (°)	90.00
q vector	1.14690(14)**a*** + 0.58921(12)**b***
Z	4
Calculated density, (g cm^{-3})	5.262
Reliable factors	
R_p/R_{wp}	0.033/0.044
R/R_w	0.033/0.024
R_m/R_{wm}	0.029/0.022
R_1/R_{w1}	0.047/0.032
Goodness of fit	1.36

Table 2
Displacement and atomic parameters of $Ag_{1/8}Pr_{5/8}MoO_4$

Atom	Site symmetry	g	x	y	z	U_{iso}, (Å^2)
Pr/Ag[a]	*4e*	0.75	1/2	3/4	0.1289 (8)	0.026 (3)
Mo	*4e*	1	1/2	3/4	0.6256 (5)	0.0426 (11)
O1	*8f*	1	0.3842 (16)	0.023 (3)	0.7195 (10)	0.014 (2)[b]
O2	*8f*	1	0.223 (2)	0.931 (3)	0.9536 (8)	0.014 (2)[b]

[a] $\Delta = 0.625$ and $x_4^0 = 0.6985$ (15) for Pr.
[b] Constrained to be equal for both oxygen atoms.

Table 3
Displacement modulation parameters of $Ag_{1/8}Pr_{5/8}MoO_4$

Atom	Parameter	A_s	A_c
Mo	x	−0.0095 (10)	0
	y	0.0097 (10)	0
	z	0	−0.0010 (9)
Pr/Ag	x	0.0105 (15)	0.034 (6)
	y	−0.0135 (14)	0.009 (6)
	z	0.0184 (16)	0.003 (1)
O1	x	0.012 (4)	0.017 (3)
	y	0.017 (5)	0.020 (5)
	z	0.007 (2)	−0.012 (2)
O2	x	0.036 (4)	0.064 (4)
	y	0.006 (3)	0.016 (4)
	z	−0.004 (2)	−0.019 (1)

Modulation function is $p = p_0 + A_s \sin 2\pi x_4 + A_c \cos 2\pi x_4$, where p—displacement parameter x, y or z, p_0—corresponding average parameter from Table 2.

Table 4
The most relevant interatomic distances of $Ag_{1/8}Pr_{5/8}MoO_4$.

Atoms	[a]Average structure (Å)	Distance range (Å)
Mo–O1 × 2	1.93 (3)	1.88–1.97
Mo–O2 × 2	1.786 (12)	1.64–1.81
Pr/Ag–O1	2.593 (11)	2.51–2.76
	2.593 (11)	2.44–2.76
	2.234 (14)	2.11–2.45
	2.234 (14)	2.01–2.48
Pr/Ag–O2	2.705 (13)	2.44–2.89
	2.705 (13)	2.62–2.78
	2.438 (13)	2.22–2.67
	2.438 (13)	1.93–2.96

[a] The average structure was refined in the space group *I*2/*b*.

3.4. High-resolution electron microscopy

HREM observations are performed at room temperature along the [001] zone axis (Fig. 8). The correspondence with the ED pattern in Fig. 3 is clear from the Fourier transform (FT) of the HREM image, inserted in Fig. 8. The structure of $Ag_{1/8}Pr_{5/8}MoO_4$ can be interpreted in terms of cation and oxygen columns viewed along the [001] direction. Usually the contrast interpretation of the HREM images is based on a comparison between the experimental and calculated images. Unfortunately, the software for the HREM image simulation for an incommensurate modulated structure is not yet available.

For this reason the simulated HREM images for $Ag_{1/8}Pr_{5/8}MoO_4$ have been calculated using the MacTempas software and the fractional coordinates of the average structure in the space group *I*2/*b* with a random distribution of Ag^+, Pr^{3+} cations and vacancies ($A = 0.125Ag^+ + 0.625Pr^{3+} + 0.25\square$). Fig. 9 shows calculated HREM images for models with a different distribution of the

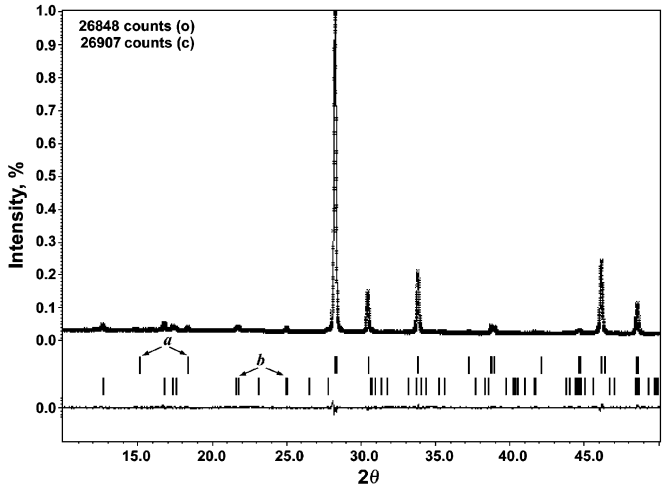

Fig. 7. Experimental, calculated and difference XRD powder patterns for $Ag_{1/8}Pr_{5/8}MoO_4$. Tick marks denote the peak positions of possible Bragg reflections for main (a) and first-order satellite (b) reflections.

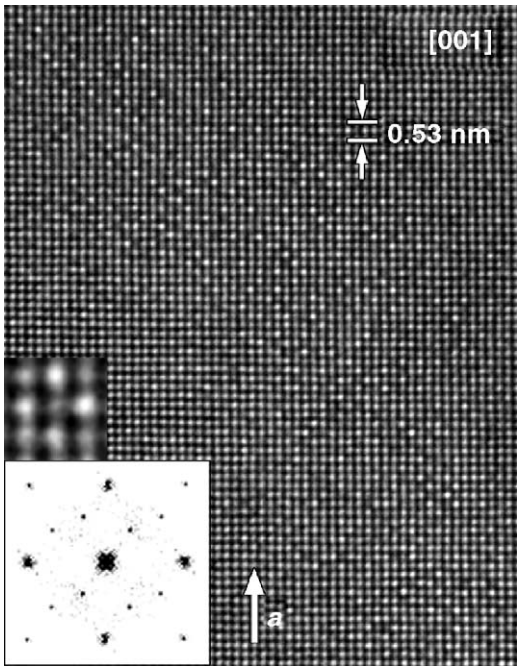

Fig. 8. [001] HREM image of the incommensurate modulated $Ag_{1/8}Pr_{5/8}MoO_4$ phase. The corresponding FT pattern and an enlargement of a square environment of a cation vacancy surrounded by brighter dots are shown as insets.

Ag^+, Pr^{3+} cations and vacancies. All dots on the [001] HREM image correspond to columns of *A* and Mo atoms (Fig. 9a). On the experimental HREM image, three types of dots with different brightness can be selected (brighter, less bright and the least bright) (Fig. 8) while this difference in the brightness of the dots is not observed in the calculated images of Fig. 9a.

It is logical to assume that the brightness difference of the dots is the result of vacancy and cation ordering. Therefore the fractional coordinates of the average structure in the space group *I*2/*b* were transformed into a

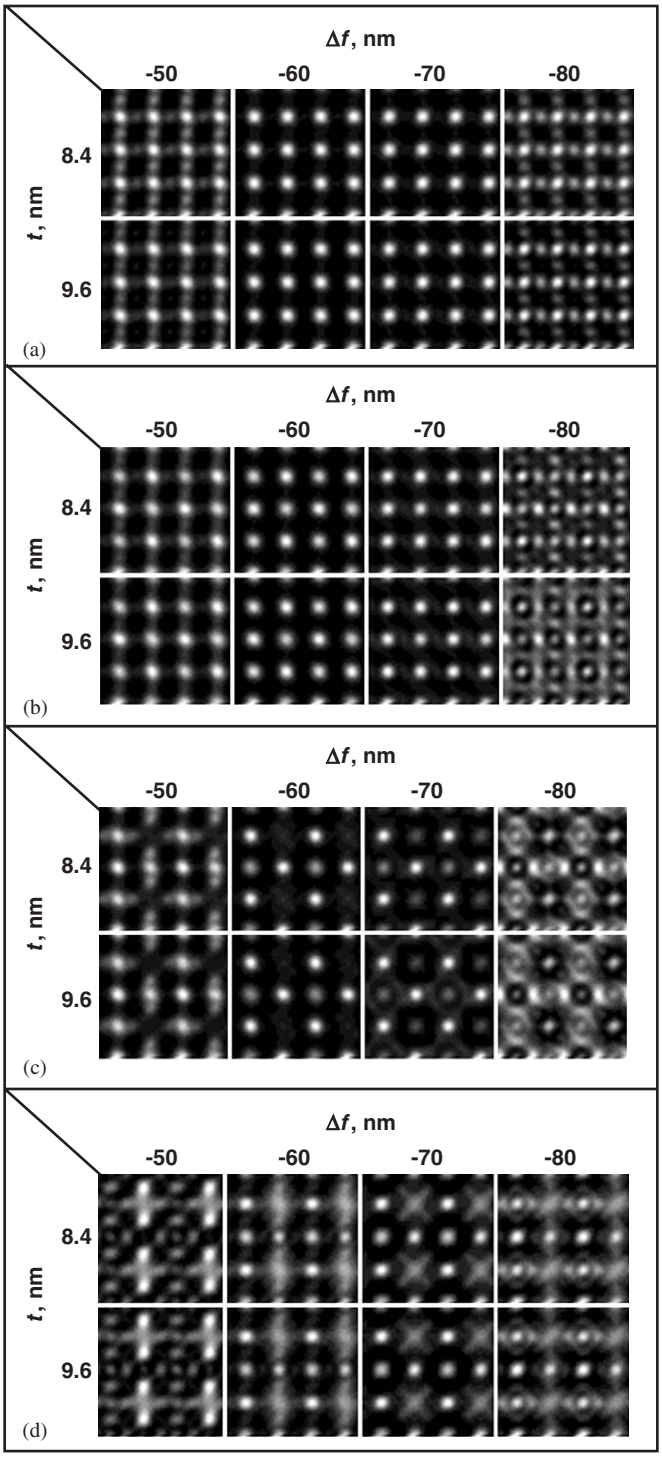

Fig. 9. Matrix of simulated [001] high-resolution images for different defocus (Δ*f*) and thickness (*t*) values assuming different structural models of $Ag_{1/8}Pr_{5/8}MoO_4$ with a different distribution of the Ag^+, Pr^{3+} cations and vacancies: (a) average structure; (b) Ag^+ and Pr^{3+} cations; (c) Pr^{3+} cations and vacancies; (d) Ag^+, Pr^{3+} cations and vacancies.

P1 lattice. In this case, all the atoms in the structure occupy independent positions and the influence of the vacancy and cation distribution can be observed in the brightness of the dots on the calculated HREM image. Slight differences on the HREM image have been observed between columns of

Pr and Ag atoms (Fig. 9b) while the vacancy cation order leads to an increase of the brightness difference (Fig. 9c and d). Brighter dots and small intensity dots on the [001] HREM image correspond to columns with Pr (Fig. 9c)/Ag (Fig. 9d) atoms and vacancies, respectively. In both cases the medium bright dots correspond to columns with only Pr atoms.

In the [001] experimental HREM image, clear regions with a square environment of a column with a cation vacancy surrounded by brighter dots can be discerned (see inset Fig. 8).

4. Discussion

A new complex silver praseodymium molybdenum oxide $Ag_{1/8}Pr_{5/8}MoO_4$ has been synthesized by a solid-state method and studied by X-ray powder diffraction and electron microscopy. $Ag_{1/8}Pr_{5/8}MoO_4$ is based on the scheelite-type structure. The substitution of Ca^{2+} by Ag^{+} and Pr^{3+} cations in $CaMoO_4$ leads to the formation of cation vacancies in the framework and the formula of the silver praseodymium molybdenum oxide should be more correctly written as $Ag_{1/8}Pr_{5/8}\square_{1/4}MoO_4$; one-fourth of the cation positions being vacant. The ordering of these cation vacancies is the reason of the structural modulation.

Transmission electron microscopy revealed that the real structure of $Ag_{1/8}Pr_{5/8}MoO_4$ requires a (3 + 1)D approach with superspace group $B2/b(\alpha\beta0)00$ (unique axis c), with a modulation vector having approximate components $\mathbf{q} = 0.56\mathbf{a}^* + 0.59\mathbf{b}^*$. The incommensurately modulated structure of $Ag_{1/8}Pr_{5/8}MoO_4$ has been solved and refined by the Rietveld method from X-ray powder diffraction data using the superspace group $I2/b(\alpha\beta0)00$ ($\mathbf{q} = 1.14690(14)\mathbf{a}^* + 0.58921(12)\mathbf{b}^*$). Most probably, $Ag_{1/8}Pr_{5/8}MoO_4$ is the first representative in a large family of incommensurately modulated scheelite-type compounds with general composition $M_{1/8}R_{5/8}\square_{1/4}MoO_4$ (M = monovalent cations; R = trivalent cations). The $Ag_{1/8}Pr_{5/8}MoO_4$ structure can be considered as consisting of groups of five AO_8 (A = Pr, Ag) polyhedra, alternating with two cation vacancies (e.g. left part of Fig. 10, along a vertical line). This vacancy order creates a superlattice with lattice parameters $\mathbf{A} = 3\mathbf{a} + \mathbf{b}$, $\mathbf{B} = -\mathbf{a} + 2\mathbf{b}$ indicated in Fig. 10 by a full line. The incommensurately modulated structure can then be described as a shear structure with displacement vector $\mathbf{R} = [100]_{CaMoO_4}$ or $\frac{1}{7}[2\,\bar{1}\,0]$ in the **A**, **B** ordered structure. At the interface the (five AO_8 polyhedra + two vacancies) order is distorted by the formation of only one vacancy. A preliminary investigation showed the existence of a Pr/Ag homogeneity region. Taking into account the possibility of a homogeneity range, the most general composition can be represented as $M_{x/8}R_{(16-x)/24}\square_{(4-x)/12}MoO_4$. This composition is calculated using (i) charge compensation $x + 3y = 16$ and (ii) the number of atoms in A site $x + y + z = 8$ (where x, y, z—integer) for the general composition $M_xR_y\square_z(MoO_4)_8$. The $M_{x/8}R_{(16-x)/24}\square_{(4-x)/12}MoO_4$ presentation is very comfortable and allows to describe all scheelite-type phases formed in the region between $MLn(MoO_4)_2$ ($x = 4$) and $Ln_2(MoO_4)_3$ ($x = 0$) (M = alkali metal, Ag; $R = Ln$, Y, Bi).

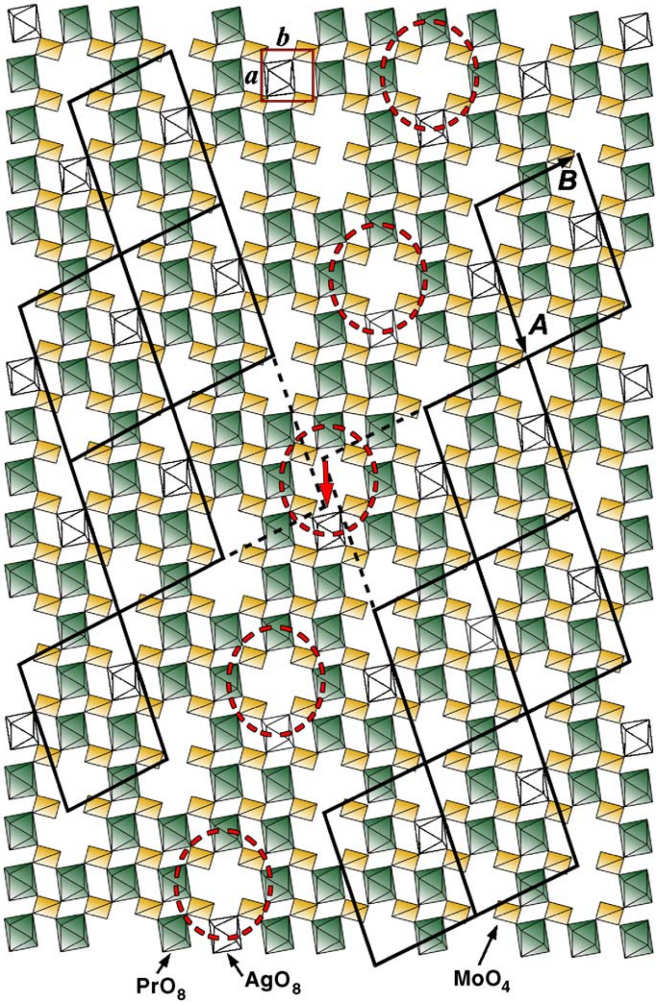

Fig. 10. Model of a layer in the modulated $Ag_{1/8}Pr_{5/8}MoO_4$ structure. The $I2/b$ setting is indicated by a square. The vacancy order creates a superlattice (outlined by the full lines) that is distorted at the interface by the formation of only one vacancy (dashed circles). The arrow indicates the displacement vector **R** of the shear structure. Displacement modulations are not included.

The observed modulation is incommensurate, while the proposed (idealized) model can be either commensurate or incommensurate. Indeed, the model does not take into account minor displacement modulations, nor a variation in the number of vacancies.

An incommensurate modulation in the scheelite-type compounds $La_{1-x}Th_xNbO_{4+x/2}$ and $LaNb_{1-x}W_xO_{4+x/2}$ was first observed by Cava et al. [36]. In both $LaNbO_4$–$ThNbO_{4.5}$ and $LaNbO_4$–$LaWO_{4.5}$ systems, the incommensurately modulated phase exists over a significant range of oxygen excess ABO_{4+x} compounds. Two main reasons can be at the origin of such structural modulation: either a fluctuation around the average composition (occupancy modulation), or a displacement of atoms from their

average positions (displacive modulation). Often a combination of both is observed and for scheelite-type compounds indeed both effects are found. A displacive modulation takes place in the oxygen excess ABO_{4+x} compounds while a composition fluctuation is the reason for the incommensurate modulation in the cation-deficient $Ag_{1/8}Pr_{5/8}MoO_4$ phase.

The electrical conductivity measurements of the $La_{1-x}Th_xNbO_{4+x/2}$ phases have shown that conductivity in the modulated phases is several orders of magnitude larger than in the $LaNbO_4$ [36]. But conductivity decreases with increasing oxygen content within the modulated phase. Probably the modulation of cations and vacancies in the structure of cation deficient $M_{1/8}R_{5/8}\square_{1/4}MoO_4$ (M = monovalent cations; R = trivalent cations) phases has its influence on the catalytic and luminescent properties of these compounds.

Acknowledgments.

The authors are grateful to A.V. Arakcheeva (Laboratoire de Cristallographie, Ecole Polytechnique Fédérale de Lausanne—EPFL, Lausanne, Switzerland) and A.M. Abakumov (Department of Chemistry, Moscow State University) for useful discussions. This work has been perfomed within the framework of IAP V-1 of the Belgian government.

References

[1] (a) H.M. Pask, J.A. Piper, IEEE J. Quant. Electron. 36 (2000) 949;
(b) A.S. Grabtchikov, A.N. Kuzmin, V.A. Lisinetskii, V.A. Orlovich, G.I. Ryabtsev, A.A. Demidovich, Appl. Phys. Lett. 75 (1999) 3742;
(c) T.T. Basiev, A.A. Sobol, P.G. Zverev, V.V. Osiko, R.C. Powell, Appl. Opt. 38 (1999) 594;
(d) P. Cerny, H. Jelinkova, T.T. Basiev, P.G. Zverev, IEEE J. Quant. Electron. 38 (2002) 1471.

[2] (a) S. Neeraj, N. Kijima, A.K. Cheetham, Chem. Phys. Lett. 387 (2004) 2;
(b) K. Shimamura, H. Sato, A. Bensalah, H. Machida, N. Sarukura, T. Fukuda, Opt. Mater. 19 (2002) 109;
(c) Z. Cheng, Q. Lu, S. Zhang, J. Liu, X. Yi, F. Song, Y. Kong, J. Han, H. Chen, J. Cryst. Growth. 222 (2001) 797;
(d) F. Shi, J. Meng, Y. Ren, Q. Su, J. Phys. Chem. Solids. 59 (1998) 105.

[3] R.M. Hazen, L.W. Finger, J.W.E. Mariathasan, J. Phys. Chem. Solids. 46 (1985) 253.

[4] V.K. Trunov, V.A. Efremov, Yu.A. Velikodny, Crystallography and Properties of Double Molybdates and Tungstenates, Nauka, Leningrad, 1986 (in Russian).

[5] A.A. Evdokimov, V.A. Efremov, V.K. Trunov, Compounds of the Rare Earth Elements, Nauka, Moscow, 1991 (in Russian).

[6] (a) P.V. Klevtsov, R.F. Klevtsova, Sov. Zh. Strukt. Chem. 18 (1977) 419 (in Russian);
(b) P.V. Klevtsov, R.F. Klevtsova, Sov. J. Struct. Chem. 18 (1977) 339 (Engl. Transl.).

[7] P.V. Klevtsov, V.I. Protasova, L.Yu. Kharchenko, R.F. Klevtsova, Crystallography Reports 18 (1973) 833 (in Russian).

[8] Hk. Müller-Buschbaum, T. Gressling, J. Alloys Compd. 201 (1993) 267.

[9] A.W. Sleght, K. Aykan, D.B. Rogers, J. Solid State Chem. 13 (1975) 231.

[10] M. Rath, Hk. Müller-Buschbaum, J. Alloys Compd. 198 (1993) 193.

[11] A.M. Golub, A.P. Perepelitsa, N.S. Slobodyanik, P.P. Popel, Russ. J. Inorg. Chem. 21 (1976) 1142 (in Russian).

[12] A.P. Perepelitsa, V.I. Ishchenko, I.Ya. Pichay, Russ. J. Inorg. Chem. 36 (1991) 485 (in Russian).

[13] F. Shi, J. Meng, Y. Ren, Mater. Res. Bull. 30 (1995) 1401.

[14] F. Shi, J. Meng, Y. Ren, J. Alloys Compd. 233 (1996) 56.

[15] F. Shi, J. Meng, Y. Ren, J. Solid State Chem. 121 (1996) 236.

[16] A.P. Perepelitsa, Zh. Prikl. Khim. 69 (1996) 1252 (in Russian).

[17] G.W. Keulks, L.D. Krenzke, T.M. Noterdam, Adv. Catal. 27 (1978) 183.

[18] J.F. Brazdil, D.D. Suresh, R.K. Grasselli, J. Catal. 66 (1980) 347.

[19] R.K. Grasselli, J.D. Burlington, Adv. Catal. 30 (1981) 133.

[20] Y.-H. Han, W. Ueda, Y. Moro-Oka, J. Catal. 186 (1999) 75.

[21] A.F. Van den Elzen, G.D. Rieck, Acta Crystallagr. 29 (1973) 2433.

[22] K. Aykan, A.W. Sleight, D.B. Rogers, J. Catal. 29 (1973) 185.

[23] J.F. Brazdil, L.C. Glaeser, R.K. Grasselli, J. Catal. 81 (1983) 142.

[24] J.F. Brazdil, R.K. Grasselli, J. Catal. 79 (1983) 104.

[25] W. Jeitschko, Acta Crystallogr. B 29 (1973) 2074.

[26] D.H. Templeton, A. Zalkin, Acta Crystallogr. 16 (1963) 762.

[27] M. Gärtner, D. Abeln, A. Pring, M. Wilde, A. Reller, J. Solid State Chem. 111 (1994) 128.

[28] T.P. Rybakova, V.K. Trunov, Russ. J. Inorg. Chem. 19 (1974) 1631 (in Russian).

[29] V.K. Trunov, A.A. Evdokimov, T.P. Rybakova, T.A. Berezina, Russ. J. Inorg. Chem. 24 (1979) 168 (in Russian).

[30] R.W.G. Wyckoff, J. Amer. Chem. Soc. 44 (1922) 1994.

[31] Powder Diffraction File, Card 08-0473, JCPDS; International Centre for Diffraction Data, 1601 Park Lane, Swarthmore, PA 19081.

[32] V. Petricek, M. Dusek, JANA2000: Programs for Modulated and Composite Crystals, Institute of Physics, Praha, Czech Republic, 2000.

[33] T. Janssen, A. Janner, A. Looijenga-Vos, P.M. de Wolff, Incommensurate and commensurate modulated structures, in: A.J.C. Wilson (Ed.), International Tables for Crystallography, Vol. C, Kluwer Academic Publishers, Dordrecht, 1995, pp. 797–835.

[34] P.M. De Wolf, Acta Crystallogr. A 30 (1974) 777.

[35] P.M. De Wolf, T. Jansen, A. Janner, Acta Crystallogr. A 37 (1981) 625.

[36] R.J. Cava, R.S. Roth, T. Negas, H.S. Parker, D.B. Minor, J. Solid State Chem. 40 (1981) 318.